

Improved Charge Collection via Sulphur Doping on Bismuth Iodide Thin Films for Photovoltaic Application

Bowon Yoo¹, Dong Ding¹, Jose M. Marin-Beloqui¹, Luis Lanzetta¹, Xiangnan Bu¹, Thomas Rath² and Saif. A. Haque^{1*}

¹ Department of Chemistry and Centre for Plastic Electronics, Imperial College London, South Kensington Campus, London SW7 2AZ, United Kingdom

² Institute for Chemistry and Technology of Materials, NAWI Graz, Graz University of Technology, Stremayrgasse 9, 8010 Graz, Austria

KEYWORDS : *Bismuth Iodide, Photovoltaics, TAS*

ABSTRACT: Stable and non-toxic bismuth iodide, which can address the intrinsic problems of lead based perovskites, has become one of emerging promising materials for solar cell active layer with its prospective optical properties such as narrow band gap (1.7 eV) and high absorption coefficient (10^5 cm^{-1}) in the visible region. Despite these promising features, solar cells employing this material has only achieved around 1% yet which is quite far apart from the theoretical limitation from its band gap, 28%. This unsatisfactory efficiency may come from its very short carrier lifetimes (180-240 ps) and therefore, efficient separation of mobile charges is necessary. It is found in this paper that formation of bismuth sulfur iodide between ETL and the bismuth iodide active layer helps to have more efficient charge separation through transient optical spectroscopy studies. However, due to the low lying conduction band of the bismuth sulfur iodide layer, it was needed to find appropriate ETL to match the energy level and a device with the optimized structure performed with 1.21% power conversion efficiency.

Introduction

Solar cells employing organic-inorganic hybrid lead perovskites, APbX_3 , are now one of the most attractive alternatives to conventional solar cells, as they are achieving an efficiency spur from 3.8% to 22.7%.¹ This rapid improvement in efficiency in only a few years has been resulted from the rapid progress including processing conditions², device architectures^{3,4} and precursor chemistries⁵. However, there are two intrinsic problems to be solved, the toxicity of lead and the instability of lead based perovskite structure.^{6,7} In order to address these concerns, several alternative materials have been suggested. Especially, investigations on air-stable and lead-free perovskites such as tin(IV) based perovskite⁸, bismuth based perovskite⁹ and halide double perovskite¹⁰ have been conducted by several groups, expecting advantages in optical characteristics from the perovskite structure. However, those air-stable and lead-free perovskites have not achieved more than 2% of power conversion efficiency (PCE) yet, and the highest is only 1.64%¹⁰ until now. Therefore, researchers are still finding other air-stable and lead-free alternatives.

In that view, all-inorganic metal-halides, for example, bismuth iodide (BiI_3) can be a prospective candidate for the light absorber in a solar cell.¹¹ Bismuth is becoming one of the most popular lead replacement with chemical similarity and similar density.¹² It has a $[\text{Xe}]4f^{14}5d^{10}6s^2$ electronic configuration like

lead and this configuration make bismuth has resistance to oxidation due to the presence of an inert $6s^2$ electron pair.¹³ The crystal structure of BiI_3 is rhombohedral crystal structure (space group $R\bar{3}$)¹⁴ where a layered 2D structure is built from BiI_6 octahedra with the iodide atoms occupying a hexagonal close-packed lattice and bismuth atoms occupying 2/3 of the octahedral sites between every second layer.¹⁵

BiI_3 had been commonly researched for the application as an X-ray detector due to its large X-ray cross-section availability from large nuclear mass.¹⁶ After first application of this material in a solar cell as a hole transport material (HTM) in organic solar cells,¹⁷ it has been attracting the interest for the photovoltaic (PV) application with its suitable optical properties as follows.¹⁸⁻²⁰ The band gap value of BiI_3 which is indirect is $\sim 1.7 \text{ eV}$,^{19,20} and it has high absorption coefficient, which is higher than 10^5 cm^{-1} , in the visible region.²⁰ Solution process availability is another merit of BiI_3 has for the massive production.^{11,19} Taking advantage from such properties, this material was applied as an active layer in solar cells with organic HTL by Lehner *et al.*, but the cells were able to achieve only 0.35% of PCE.¹⁹ This work showed the potentiality of BiI_3 in PV application, but the low efficiency may come from lack of understanding on the material chemistry on the material itself and suboptimal components and structure of devices. Especially, the generated charges on BiI_3 have relatively short lifetime,

180-240 ps, resulting in charges recombining before being transferred to electrodes.²⁰ Scholz et al.²¹ observed not only the short life time of generated charges but also the presence of strong electron-phonon coupling in BiI_3 which can result in self-trapped excitons.²² Therefore, the optimisation of the structure is needed in order to extract charges efficiently before they recombine in the material itself. Recently, Hamdeh et al.¹¹ improved PCE from 0.32%¹⁹ to 1% by annealing under solvent vapour environment where the carrier mobility increased and forming BiOI on the surface of the active layer. However, BiOI was formed between active layer and HTM where the energy levels does not fit well. Formation of another layer for the charge extraction between ETL and active layer seems to work more efficiently, reducing number of charges lost by mismatched energy levels.

In order to achieve it, we introduced sulphur and generated bismuth sulfur iodide (BiSI) layer between ETL and BiI_3 layer, expecting more efficient charge extraction. BiSI is another air-stable and low-toxic material which has potential for the PV application.²³ Only a few papers have reported the BiSI based solar cells only achieving lower than 1% PCE.^{24,25} This material is calculated to have low conduction band,²³ however, the experimental data has not been reported yet. Here, it seems that low-lying conduction band of BiSI helps the electrons to be extracted quickly and to be sent to the ETL like TiO_2 or SnO_2 . This paper contains the research on how the thin BiSI layer was formed and how this layer enhances the electron transport and finally the efficiency of the solar cell device.

Experimental Section

Materials

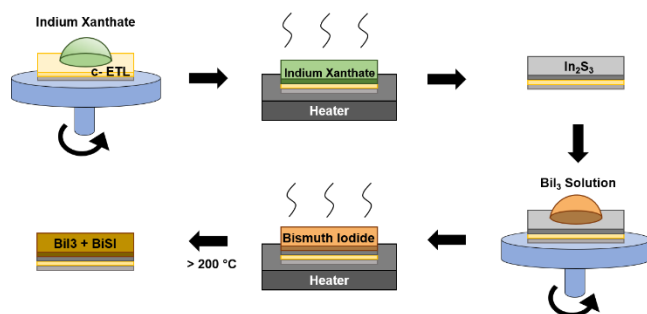


Figure 1. Schematic drawing of preparation of thin film samples of BiI_3 on substrates.

Precursors for the compact electron transport layer (ETL) were spin-coated onto a 1.25 mm × 1.25 mm substrate, resulting in a thin film. On the top of the prepared film, 134 mg/ml indium xanthate solution in chlorobenzene was deposited and then annealed at 200 °C for 15 min in a N_2 filled glove box to form an indium sulfide (In_2S_3) compact layer for sulfur supply.²⁶ On this In_2S_3 compact layer a prepared 200 mg/mL BiI_3 solution in anhydrous dimethylformamide (DMF) was spin-coated and then annealed at 100 or 200 °C for 20 min. In the case of the film annealed at 200 °C, BiSI and BiI_3 mixed layer was formed. The whole process is illustrated in figure 1. For charge carrier dynamics study between layers, spiro-OMeTAD was applied as a hole transport layer (HTL) on the top of this

film. More detailed procedure can be found in the supporting information.

For PV devices, commercial fluorine indium tin oxide-coated (ITO) glass substrates were used as the substrates. The ITO glass substrates were cleaned in consecutive ultrasounds bath in soap, deionised water, acetone and isopropanol in order, for 20 min each then dried by N_2 blowing and heated in the oven. The compact ETL, In_2S_3 , BiI_3 active layer and HTL were prepared through the same process for the thin film preparation above. Finally, 100 nm of Ag was thermal evaporated at the pressures not higher than 5E-6 Bar as a backside electrode. The films were stored in the ambient condition without illumination for 14 days to oxidise spiro-OMeTAD. The detailed procedure is in supporting information.

Crystallographic Properties were investigated using X-ray diffraction (XRD) with a PANalytical X'Pert Pro MRD diffractometer equipped with a Ni filtered $\text{Cu K}\alpha$ X-ray at 40 kV and 40 mA. The data of 2θ degree between 12.5° to 60° was obtained and samples were mounted in a top-loaded trough and it rotated during data collection. BiI_3 films deposited on substrates prepared following the procedure in materials part above.

Scanning electron microscopy (SEM) images of the prepared BiI_3 films were taken from LEO Gemini 1525 high resolution field emission gun SEM (Zeiss) which was fitted with Oxford Instruments INCA energy dispersive and wavelength dispersive x-ray spectrometers, after the films loaded on a conductive carbon tape and 10nm chromium film sputtered on them by using Q150T Turbo-Pumped Sputter Coater.

UV-Vis Spectra was obtained from a Shimadzu 2600 spectrophotometer including an ISR-2600Plus integrating sphere attachment.

Transient Absorption Spectroscopy (TAS) was employed for the investigation on time related electro chemical processes. The samples under nitrogen atmosphere were excited by a pump light source (laser excitation energy density: $\sim 15 \mu\text{J}\cdot\text{cm}^{-2}$), a nitrogen laser (Photon Technology International Inc. GL-3300) shooting at a dye laser (Photon Technology International Inc. GL-301). A probe light, which was generated by a quartz halogen lamp (100 W; Bentham, IL 1) powered through Bentham 605 supply unit, passed through the excited samples and then electronic band-pass filters (Costronic Electronics), and the probe light was detected with light detectors (Si-photodiodes; Hamamatsu Photonics, S1722-01). The TAS signals were amplified by a digital oscilloscope (Tektronics, DPO3012), and they were collected and synchronized with a trigger signal from the pump laser pulse from a photodiode (Thorlabs Inc., DET210). According to the absorption spectrum (figure 2), the wavelength of the pump laser was set at 510 nm for BiI_3 thin films and the wavelength of continuous probe light was set from 1000 nm to 1600 nm.

JV characterisations of the fabricated solar cell devices were conducted by illumination ($100 \text{ mW}\cdot\text{cm}^{-2}$) and measurement of the current change as different bias applied by a LCS-100TM solar simulator system with a 150 W xenon lamp which was calibrated with a standard Silicon solar cell.

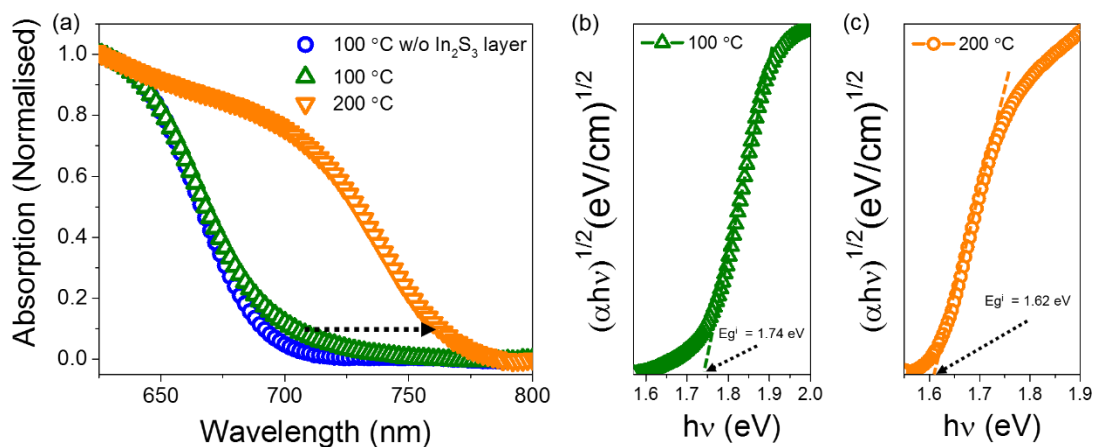


Figure 2. Normalized UV-Vis absorption spectra of BiI_3 on In_2S_3 layer annealed at different temperatures and Tauc plots for the film annealed at b) 100 °C and c) 200 °C, giving the band gaps.

Results and Discussion

When BiI_3 film was annealed on indium sulfide layer, the red-shifted absorption spectrum was obtained as shown in figure 2 (a). Annealing at low temperature (100 °C) did not change its band gap and the film without while annealing at high temperature (200 °C) changed its optical property much. Not shown in the figure, but when the film without In_2S_3 under layer was annealed at 200 °C, the film became almost transparent as reported by Hamdeh et al.¹¹ The reason for the shift of the band gap is expected to be the formation of BiSI from the reaction between BiI_3 and In_2S_3 as confirmed by XRD below.

We obtained the absorption coefficient (α) from transmittance (T), reflectance (R), and the thickness of the sample (d).

$$\alpha = \frac{-\ln(T/(1-R))}{d} \quad (1)$$

Assuming an indirect bandgap as following the literature,^{15,23} the Tauc method was applied to find a linear absorption edge (figure 2 (b) and (c)). The bandgaps were determined to be 1.74^{19,20} and 1.62²³ eV for the annealing at 100 °C and 200 °C, respectively where the bandgap matches with the previous reported band gaps of BiI_3 and BiSI .

The film with low-temperature annealing has the absorption coefficient (α) higher than 10^5 cm^{-1} above 1.9 eV (650 nm) which coincides with the result from the previously reported.²⁷ Otherwise, in the case of the film annealed at higher temperature, its absorption coefficient is higher than 10^5 cm^{-1} above 1.75 eV (710 nm) where it can absorb larger range of the light with fairly high absorption coefficient.

Figure 3 is the collected XRD patterns and a relevant reference in order to confirm the formation of BiSI by annealing at 200 °C. The XRD pattern from the 100 °C annealed film, there are only the peaks for BiI_3 (figure S1) while the pattern from the 200 °C annealed film, there are not only peaks for BiI_3 but also peaks for BiSI . The peaks marked with stars can be assigned to the peaks from BiSI (figure 3 (c)). To confirm whether the BiSI peaks from the reaction between BiI_3 and

In_2S_3 , the XRD patterns of each powders and their powder mixture heated at 200 °C were also obtained (figure S1). The powders were heated in the nitrogen filled glove box to prevent reactions with other components of the ambient air. In the pattern of powder mixture, peaks for BiSI appeared as well and therefore it can be concluded that BiSI was formed during the annealing.

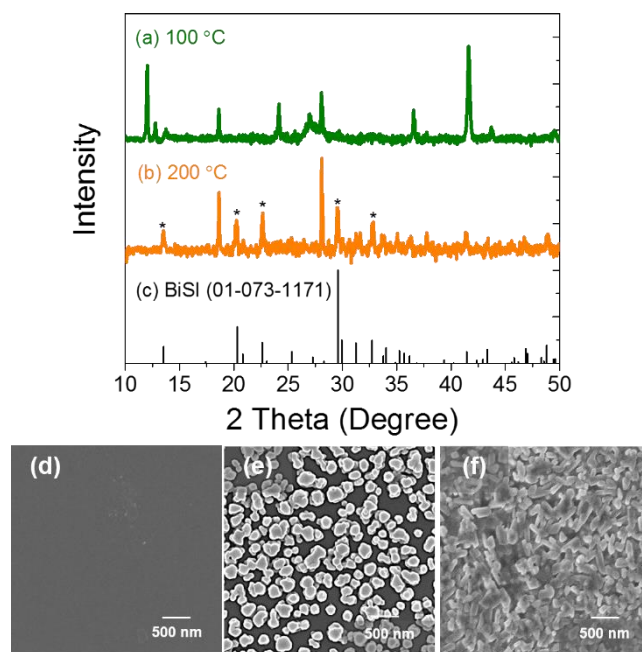


Figure 3. X-ray diffraction patterns of BiI_3 films on In_2S_3 annealed at (a) 100 °C and (b) 200 °C respectively and (c) the references of BiSI (code: 01-073-1171). SEM images of (d) In_2S_3 , $\text{BiI}_3/\text{In}_2\text{S}_3$ annealed at (e) 100 °C and (f) 200 °C and on c- $\text{TiO}_2/\text{glass}$ substrates.

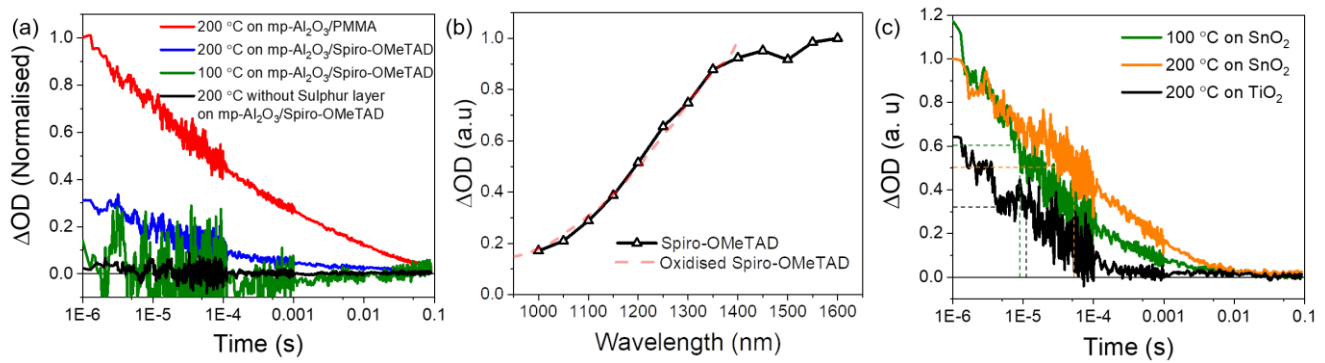


Figure 4. (a), (c) Time-resolved transient absorption spectrums of BiI_3 thin films in different structure at 1600 nm and (b) transient absorption spectra of Spiro-OMeTAD/ BiI_3 / In_2S_3 / TiO_2 /glass thin films at 10 μs after pulsed and absorption spectrum of chemically oxidised Spiro-OMeTAD chemically oxidised with $N(PhBr)_3SbCl_6$.

This reaction between BiI_3 and In_2S_3 affected morphology of the BiI_3 thin film as well, as can be seen in SEM images above. Figure 3 (d) shows compactly and evenly formed In_2S_3 layer on the glass substrate. With low temperature annealing, deposited BiI_3 nano-crystals remained, not covering whole the surface with many defects (figure 3 (e)). However, in figure 3 (f), it is observed that the particles are covering whole the surface with much less defects. Considering both XRD patterns and SEM images, the formation of the BiSI in the film during the annealing with high enough temperature as expected with absorption spectra and the film became the mixture of BiI_3 and BiSI. This led the film to have compact and homogeneous morphology which is desired to solar cell active layer.

Figure 4 (a) shows TAS signals from the different BiI_3 films structures. First, without Spiro-OMeTAD any obvious decay was not observed during the measurement. The reason for it is that the observed decay at 1600 nm is the decay of generated polarons in Spiro-OMeTAD. It becomes clearer with Figure 4 (b), the transient absorption spectra, it matches with the absorption spectrum of chemically oxidised Spiro-OMeTAD.²⁸ Therefore, all the other TAS signals were obtained with Spiro-OMeTAD. Comparing the films annealed at two different temperatures, the film annealed at higher temperature gave three times higher signal. It means almost three times of Spiro-OMeTAD polarons were remained until micro-time scale after pulsed. Without In_2S_3 layer, there was no signal although it was annealed at 200 °C, meaning none of the polarons survived until this time scale. If there is no In_2S_3 , the electrons generated in BiI_3 cannot go to anywhere in Al_2O_3 / BiI_3 /PMMA structure and therefore, they may recombine with holes in BiI_3 or transferred holes on Spiro-OMeTAD and it happens in quicker than a micro second. However, when there is In_2S_3 , the electrons can go to In_2S_3 layer and the concentration of electrons in BiI_3 becomes lower. So, there is less amount of recombination of holes and electrons in the BiI_3 layer itself and higher chance to the holes to go to Spiro-OMeTAD and live until micro-time scale as it can be seen in the figure. In the case of the film annealed at 200 °C, there is BiSI which has conduction band with low energy level where the electron transfer is more favoured. Therefore there can be more effi-

cient electron extraction before they recombined. Consequently, much higher number of remained holes can go to Spiro-OMeTAD and it results in higher signal in TAS.

When different ETMs were applied to the films it showed different decay kinetics as shown in figure 4 (c). When the film has BiSI layer after annealing on SnO_2 , the polaron decays more slowly with $\tau_{1/2} \approx 80 \mu s$, while the film without BiSI has $\tau_{1/2} \approx 8 \mu s$. When TiO_2 was applied as the ETM, even though the film had BiSI, the decay proceeded quite fast with $\tau_{1/2} \approx 12 \mu s$ and the intensity of the signal was lower.

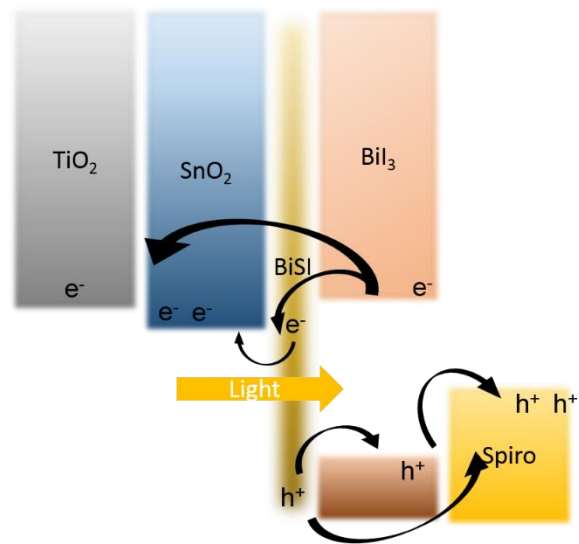


Figure 5. Schematic illustration of charge transportation process in the BiI_3 thin films. The energy levels of BiSI and BiI_3 are from literatures.^{19,23}

In general, charges are generated by light illumination. Then, the generated electrons are transferred to ETM and holes are transferred to HTM if they exist. These transferred or remained charges go through recombination pass ways: recombination of generated charges in active layer, charge back transfer at interfaces between active layer and ETM or HTM and charge back transfer between ETM and HTM. Assuming charges from BiI_3 go through the same pass ways, the process is illustrated in figure 5. Electrons could go to BiSI with low

conduction band more easily than to SnO₂. Therefore, the less electrons were remained in BiI₃ and the slower charge recombination between electrons on BiI₃ and holes on spiro-OMeTAD, resulting in slower polaron decay. With TiO₂ which has higher conduction band energy level, the smaller number of electrons were transferred to TiO₂, and therefore the recombination became faster than the film with SnO₂.

The longer lived polarons and higher amount of the signal mean that there is a higher chance to be collected to the electrode in a solar cell system. Devices were fabricated with the same structure that TAS conducted to investigate the effect of the inter-layer in the device performance.

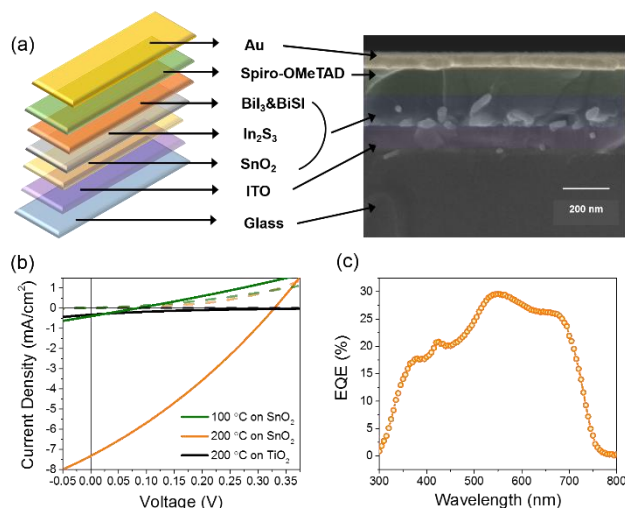


Figure 6. BiI₃ solar cell devices annealed at different temperatures and with c-SnO₂ or c-TiO₂ as the ETM. (a) Schematic device architecture and (b) cross-sectional SEM image, (c) JV traces of the assembled devices (dash lines are under dark) and (d) external quantum efficiency.

The structure of the fabricated solar cell is illustrated in figure 6 (a) and its cross-sectional SEM image is in figure 6 (b). Figure 6 (c) shows the JV traces if the fabricated solar cell devices. Obtained values including J_{sc}, V_{oc}, FF and PCE of devices are listed on table 1. The device with 100 °C annealing did not achieve high enough V_{oc} nor J_{sc}. This may come from the charge recombination in BiI₃ without being transferred to the ETL or HTL efficiently. In the presence of BiSI with 100 °C annealing, charges were quickly transferred from active layer to the layer formed and therefore longer-lived charges could be extracted to the electrode showing higher V_{oc} and J_{sc} with 0.7% PCE. In the case of TiO₂, maybe the charges transferred to BiSI could not be transferred to TiO₂ due to the energy level mismatch. Further study is need for the exact energy level of BiSI to confirm it. Figure 6 (d) shows EQE that the most of charges were from the active layer, exactly matching with the absorption spectrum in figure 2.

Figure 7 is the JV trace of the champion device with the structure in figure 6 (a). Solar cells applied BiI₃ have achieved 1%,^{11,19,29} and the cells with BiSI have achieved 0.7% until now.^{24,25} This annealing method to improve charge collection efficiency with formation of BiSI achieved higher PCE of 1.21% and the average PCE of 0.64 ± 0.25 %. The histogram of 45 device pixels can be found in figure S3.

Table 1. Summary of photovoltaic performance of devices from different structures and annealing temperatures.

| | V _{oc} (V) | J _{sc} (mA/cm ²) | FF | PCE (%) |
|----------------------------|---------------------|---------------------------------------|------|---------|
| 100 °C on SnO ₂ | 0.08 | 0.40 | 0.25 | 0.01 |
| 200 °C on SnO ₂ | 0.33 | 7.32 | 0.30 | 0.72 |
| 100 °C on TiO ₂ | 0.49 | 0.32 | 0.12 | 0.02 |

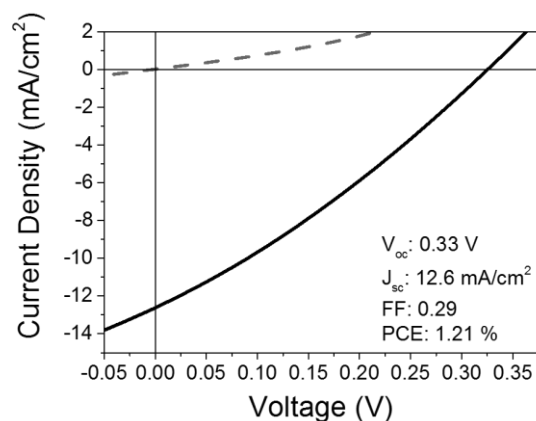


Figure 7. JV traces of the assembled device which gave the highest efficiency.

To conclude, an additional layer of BiSI was generated to enhance charge extraction efficiency to prevent quick charge recombination which is intrinsic characteristic of BiI₃. This layer enhanced the number of electrons and holes that reach the electrodes in a device, improving average PCE to become 0.64% and the best PCE of 1.21%. This achievement is in a planar structure without mesoporous(mp) ETL. mp-TiO₂ which is one of most popularly used mp-ETL cannot be applied here, for the energy level of TiO₂ seems not to match with BiSI. Therefore, if mp-SnO₂ or any other mp-ETL with lower conduction band can be applicable, it is expected to bring higher PCE. Additionally, different HTLs with lower valence band are expected to give higher V_{oc}. Thus, there is still much room for improvement with and further research is required.

ASSOCIATED CONTENT

(Word Style “TE_Supporting_Information”). **Supporting Information.** A brief statement in nonsentence format listing the contents of material supplied as Supporting Information should be included, ending with “This material is available free of charge via the Internet at <http://pubs.acs.org>.” For instructions on what should be included in the Supporting Information as well as how to prepare this material for publication, refer to the journal’s Instructions for Authors.

AUTHOR INFORMATION

Corresponding Author

* (Word Style “FA_Corresponding_Author_Footnote”). Give contact information for the author(s) to whom correspondence should be addressed.

Present Addresses

†If an author’s address is different than the one given in the affiliation line, this information may be included here.

Author Contributions

The manuscript was written through contributions of all authors. / All authors have given approval to the final version of the manuscript. / ‡These authors contributed equally. (match statement to author names with a symbol)

Funding Sources

Any funds used to support the research of the manuscript should be placed here (per journal style).

Notes

Any additional relevant notes should be placed here.

ACKNOWLEDGMENT

(Word Style "TD_Acknowledgments"). Generally the last paragraph of the paper is the place to acknowledge people (dedications), places, and financing (you may state grant numbers and sponsors here). Follow the journal's guidelines on what to include in the Acknowledgement section.

ABBREVIATIONS

REFERENCES

(Word Style "TF_References_Section"). References are placed at the end of the manuscript. Authors are responsible for the accuracy and completeness of all references. Examples of the recommended formats for the various reference types can be found at <http://pubs.acs.org/page/4authors/index.html>. Detailed information on reference style can be found in The ACS Style Guide, available from Oxford Press.

(1) Laboratory, N. R. E. Best Research-Cell Efficiencies. <https://www.nrel.gov/pv/assets/images/efficiency-chart.png> (Oct 30 2017).

(2) Jeon, N. J.; Noh, J. H.; Kim, Y. C.; Yang, W. S.; Ryu S.; Seok S. I. Solvent engineering for high-performance inorganic-organic hybrid perovskite solar cells, *Nat. Mater.*, **2014**, *13*, 897-903.

(3) Lee, M. M.; Teuscher, J.; Miyasaka, T.; Murakami, T. N.; Snaith, H. J. Efficient Hybrid Solar Cells Based on Meso-Superstructured Organometal Halide Perovskites, *Science*, **2012**, *338*, 643-647.

(4) Park, N. Perovskite solar cells: an emerging photovoltaic technology, *Materials Today*, **2015**, *18*, 65-72.

(5) Zhou, Y.; Yang, M.; Wu, W.; Vasiliev, A. L.; Zhu, K.; Padture, N. P. Room-temperature crystallization of hybrid-perovskite thin films via solvent-solvent extraction for high-performance solar cells., *J. Mater. Chem. A*, **2015**, *3*, 8178-8194.

(6) Babayigit, A.; Ethirajan, A.; Muller, M.; Conings, B. Toxicity of organometal halide perovskite solar cells, *Nat. Mater.*, **2016**, *15*, 247-251.

(7) Bryant, D.; Aristidou, N.; Pont, S.; Sanchez-Molina, I.; Chotchuangchuchaval, T.; Wheeler, S.; Durrant, J. R.; Haque, S. A. Light and oxygen induced degradation limits the operational stability of methylammonium lead triiodide perovskite solar cells, *Energy Environ. Sci.*, **2016**, *9*, 1655-1660.

(8) Qiu, X.; Jiang, Y.; Zhang, H.; Qiu, Z.; Yuan, S.; Wang, P.; Cao, B. Lead free mesoscopic Cs₂NiI₆ perovskite solar cells using different nanostructured ZnO nanorods as electron transport layers, *P. Phys. Status Solidi RRL*, **2016**, *10*, 587-591.

(9) Park, B.; Philippe B.; Zhang X.; Rensmo H.; Boschloo G.; Johansson E. M. J. Bismuth Based Hybrid Perovskites A₃Bi₂I₉ (A: Methylammonium or Cesium) for Solar Cell Application, *Adv. Mater.*, **2015**, *27*, 6806-6813.

(10) Zhang, Z.; Li, X.; Xia, X.; Wang, Z.; Huang, Z.; Lei, B.; Gao, Y. High-Quality (CH₃NH₃)₃Bi₂I₉ Film-Based Solar Cells: Pushing Efficiency up to 1.64%, *J. Phys. Chem. Lett.* **2017**, *8*, 4300-4307.

(11) Hamdeh, U. H.; Nelson, R. D.; Ryan, B. J.; Bhattacharjee, U.; Petrich, J. W.; Panthani, M. G. Solution-Processed BiI₃ Thin Films for Photovoltaic Applications: Improved Carrier Collection via Solvent Annealing, *Chem. Mater.*, **2016**, *28*, 6567-6574.

(12) Cotton, F. A.; Wilkinson, G.; Murillo, C. A.; Bochmann, M.; Grimes, R. *Advanced inorganic chemistry*; Wiley: New York, **1999**; Vol. 1355.

(13) Sidgwick, N. V. *Electronic Theory of Valency*; H. Milford: 1953.

(14) Nason, D.; Keller, L. The growth and crystallography of bismuth tri-iodide crystals grown by vapor transport. *J. Cryst. Growth*, **1995**, *156*, 221-226.

(15) Mackay, R. A.; Henderson, W. *Introduction to Modern Inorganic Chemistry*, 6th ed.; CRC Press: **2002**.

(16) Lintereur, A. T.; Qiu, W.; Nino, J. C.; Baciak, J. Characterization of bismuth tri-iodide single crystals for wide band-gap semiconductor radiation detectors, *Nucl. Instrum. Methods Phys. Res., Sect. A*, **2011**, *652*, 166-169.

(17) Boopathi, K. M.; Raman, S.; Mohanraman, R.; Chou, F.; Chen, Y.; Lee, H.; b, Chang, F.; Chu, C. Solution-processable bismuth iodide nanosheets as hole transport layers for organic solar cells, *Solar Energy Materials & Solar Cells*, **2014**, *121*, 35-41.

(18) Podraza, N. J.; Qiu, W.; Hinojosa, B. B.; Xu, H.; Motyka, M. A.; Phillipot, S. R.; Baciak, J. E.; Trolier-McKinstry, S.; Nino, J. C. Band gap and structure of single crystal BiI₃: Resolving discrepancies in literature, *Journal of Applied Physics.*, **2013**, *114*, 033110.

(19) Lehner, A. J.; Wang, H.; Fabiani, D. H.; Liman, C. D.; Hébert, C.; Perry, E. E.; Wang, M.; Bazan, G. C.; Chabinye, M. L.; Seshadri, R. Electronic structure and photovoltaic application of BiI₃, *Appl. Phys. Lett.*, **2015**, *107*, 131109.

(20) Brandt, R. E.; Kurchin, R. C.; Hoye, R. L. Z.; Poindexter, J. R.; Wilson, M. W. B.; Sulekar, S.; Lenahan, F.; Yen, P. X. T.; Stevanovic, V.; Nino, J. C.; Bawendi, M. G.; Buonassisi, T. Investigation of Bismuth Triiodide (BiI₃) for Photovoltaic Applications, *J. Phys. Chem. Lett.*, **2015**, *6*, 4297-4302.

(21) Scholz, M.; Oum, K.; Lenzer, T. Pronounced exciton and coherent phonon dynamics in BiI₃, *Phys. Chem. Chem. Phys.*, **2018**, Advance Article.

(22) McCall, K. M.; Stoumpos, C. C.; Kostina, S. S.; Kanatzidis, M.G.; Wessels, B. W. Strong Electron-Phonon Coupling and Self-Trapped Excitons in the Defect Halide Perovskites A₃M₂l₉ (A = Cs, Rb; M = Bi, Sb), *Chem. Mater.*, **2017**, *29*, 4129-4145.

(23) Ganose, A. M.; Butler, K. T.; Walshcd, A.; Scanlon, D. O. Relativistic electronic structure and band alignment of BiSI and BiSeI: candidate photovoltaic materials, *Mater. Chem. A*, **2016**, *4*, 2060-2068.

(24) Hahn, N. T.; Self, J. L.; Mullins, C. B. BiSI Micro-Rod Thin Films: Efficient Solar Absorber Electrodes?, *J. Phys. Chem. Lett.*, **2012**, *3*, 1571-1576.

(25) Hahn, N. T.; Rettie, A. J. E.; Beal, S. K.; Fullon, R. R.; Mullins, C. B. n-BiSI Thin Films: Selenium Doping and Solar Cell Behavior, *J. Phys. Chem. C*, **2012**, *116*, 24878-24886.

(26) Rath, T.; Edler, M.; Haas, W.; Fischereider, A.; Moscher, S.; Schenk, A.; Trattng, R.; Sezen, M.; Mauthner, G.; Pein, A.; Meischler, D.; Bartl, K.; Saf, R.; Bansal, N.; Haque, S. A.; Hofer, F.; List, E. J. W.; Trimme, G. A Direct Route Towards Polymer/Copper Indium Sulfide Nanocomposite Solar Cells, *Adv. Energy Mater.*, **2011**, *1*, 1046-1050.

(27) Cuña, A.; Aguiar, I.; Gancharov, A.; Pérez, M.; Fornaro, L. Correlation between Growth Orientation and Growth Temperature for Bismuth Tri-Iodide Films. *Cryst. Res. Technol.*, **2004**, *39*, 899-905.

(28) O'Mahony, F. T. F.; Lee, Y. H.; Jelllett, C.; Dmitrov, S.; Bryant, D. T. J.; Durrant, J. R.; O'Regan, B. C.; Graetzel, M.; Nazeeruddin, M. K.; Haque S. A.; Improved environmental stability of organic lead trihalide perovskite-based photoactive-layers in the

presence of mesoporous TiO₂, *J. Mater. Chem. A*, **2015**, *3*, 7219-7223.

(29) Kulkarni, A.; Singh, T.; Jena, A. K.; Pinpithak, P.; Ikegami, M.; Miyasaka, T. Vapor Annealing Controlled Crystal Growth and Photovoltaic Performance of Bismuth Triiodide Embedded in Mesostructured Configurations. *ACS Appl. Mater. Interfaces*, **2018**, *10*, 9547-9554.

FIGURES (Word Style "VA_Figure_Caption"). Each figure must have a caption that includes the figure number and a brief description, preferably one or two sentences. The caption should follow the format "Figure 1. Figure caption." All figures must be mentioned in the text consecutively and numbered with Arabic numerals. The caption should be understandable without reference to the text. Whenever possible, place the key to symbols in the artwork, not in the caption. To insert the figure into the template, be sure it is already sized appropriately and paste before the figure caption. For formatting double-column figures, see the instructions at the end of the template. Do NOT modify the amount of space before and after the caption as this allows for the rules, space above and below the rules, and space above and below the figure to be inserted upon editing.

SCHEMES (Word Style "VC_Scheme_Title"). Groups of reactions that show action are called schemes. Schemes may have brief titles describing their contents. The title should follow the format "Scheme 1. Scheme Title". Schemes may also have footnotes (use Word Style "FD_Scheme_Footer"). To insert the scheme into the template, be sure it is already sized appropriately and paste after the scheme title. For formatting double-column schemes, see the instructions at the end of the template. Do NOT modify the amount of space before and after the title as this allows for the rules, space above and below the rules, and space above and below the scheme to be inserted upon editing.

CHARTS (Word Style "VB_Chart_Title"). Groups of structures that do not show action are called charts. Charts may have brief titles describing their contents. The title should follow the format "Chart 1. Chart Title". Charts may also have footnotes (use Word Style "FC_Chart_Footer"). To insert the chart into the template, be sure it is already sized appropriately and paste after the chart title. For formatting double-column charts, see the instructions at the end of the template. Do NOT modify the amount of space before and after the title as this allows for the rules, space above and below the rules, and space above and below the chart to be inserted upon editing.

TABLES. Each table must have a brief (one phrase or sentence) title that describes its contents. The title should follow the format "Table 1. Table Title" (Word Style "VD_Table_Title"). The title should be understandable without reference to the text. Put details in footnotes, not in the title (use Word Style

"FE_Table_Footer"). Do NOT modify the amount of space before and after the title as this allows for the space above and below the table to be inserted upon editing.

Use tables (Word Style "TC_Table_Body") when the data cannot be presented clearly as narrative, when many precise numbers must be presented, or when more meaningful interrelationships can be conveyed by the tabular format. Do not use Word Style "TC_Table_Body" for tables containing artwork. Tables should supplement, not duplicate, text and figures. Tables should be simple and concise. It is preferable to use the Table Tool in your word-processing package, placing one entry per cell, to generate tables.

Displayed equations can be inserted where desired making sure they are assigned Word Style "Normal". Displayed equations can only be one column wide. If the artwork needs to be two columns wide, it must be relabeled as a figure, chart, or scheme and mentioned as such in the text.

To format double-column figures, schemes, charts, and tables, use the following instructions:

- Place the insertion point where you want to change the number of columns
- From the **Insert** menu, choose **Break**
- Under **Sections**, choose **Continuous**
- Make sure the insertion point is in the new section. From the **Format** menu, choose **Columns**
- In the **Number of Columns** box, type **1**
- Choose the **OK** button

Now your page is set up so that figures, schemes, charts, and tables can span two columns. These must appear at the top of the page. Be sure to add another section break after the table and change it back to two columns with a spacing of 0.33 in.

Table 1. Example of a Double-Column Table

| Column 1 | Column 2 | Column 3 | Column 4 | Column 5 | Column 6 | Column 7 | Column 8 |
|----------|----------|----------|----------|----------|----------|----------|----------|
| | | | | | | | |

Authors are required to submit a graphic entry for the Table of Contents (TOC) that, in conjunction with the manuscript title, should give the reader a representative idea of one of the following: A key structure, reaction, equation, concept, or theorem, etc., that is discussed in the manuscript. Consult the journal's Instructions for Authors for TOC graphic specifications.

Insert Table of Contents artwork here

